ECOGRAPHY

Size matters in quantitative radar monitoring of animal migration: estimating monitored volume from wingbeat frequency

Journal:	*Ecography*
Manuscript ID	ECOG-04025.R1
Wiley - Manuscript type:	Research
Keywords:	aeroecology, environmental impact assessment, radar

Abstract:

Quantitative radar studies are an important component of studying the movement of birds. Whether a bird is detected or not depends upon its size, because the object size ultimately determines the monitored volume of a radar beam. Consequently, an accurate quantification of bird movements recorded by small-scale radar requires an accurate determination of the monitored volume for the objects in question, although this has tended to be ignored.

Here, we demonstrate the importance of sensitivity settings for echo detection on the estimated movement intensities of different sized birds. The amount of energy reflected from a bird and detected by the radar receiver (echo size) depends not only on the bird's size and on the distance from the radar antenna, but also on the beam shape and the bird’s position within this beam. We propose a method to estimate the size of a bird based on the wingbeat frequency, retrieved from the echo-signal, independent of the absolute echo size. The estimated bird-size allows calculation of size-specific monitored volumes, allowing accurate quantification of movement intensities. We further investigate the importance of applying size-specific monitored volume to quantify avian movements instead of using echo counts.

We also highlight the importance of accounting for size-specific monitored volume of small scale radar systems, and the necessity of reporting technical information on radar parameters. Applying this framework will increase the quality and validity of quantitative radar monitoring.

Journal for submission: Ecography for ENRAM special issue

Running title: *RCS via WBF*

Title

Size matters in quantitative radar monitoring of animal migration: estimating monitored volume from wingbeat frequency

Abstract

Quantitative radar studies are an important component of studying the movement of birds. Whether a bird is detected or not depends upon its size, because the object size ultimately determines the monitored volume of a radar beam. Consequently, an accurate quantification of bird movements recorded by small-scale radar requires an accurate determination of the monitored volume for the objects in question, although this has tended to be ignored.

Here, we demonstrate the importance of sensitivity settings for echo detection on the estimated movement intensities of different sized birds. The amount of energy reflected from a bird and detected by the radar receiver (echo size) depends not only on the bird's size and on the distance from the radar antenna, but also on the beam shape and the bird’s position within this beam. We propose a method to estimate the size of a bird based on the wingbeat frequency, retrieved from the echo-signal, independent of the absolute echo size. The estimated bird-size allows calculation of size-specific monitored volumes, allowing accurate quantification of movement intensities. We further investigate the importance of applying size-specific monitored volume to quantify avian movements instead of using echo counts.

We also highlight the importance of accounting for size-specific monitored volume of small scale radar systems, and the necessity of reporting technical information on radar parameters. Applying this framework will increase the quality and validity of quantitative radar monitoring.

Keywords

Avian migration, detection ranges, detection threshold, environmental impact assessment, MTR, quantitative monitoring, radar cross section, remote sensing, sensitivity time control.

Lexicon

D_{max} [m]: Maximum distance (range) of detection. At D_{max}, the echo power received from an object falls below the detection threshold $P_{r_{min}}$. D_{max} primarily depends on the object's RCS, and radar properties such as the transmitted power P_t and antenna gain G_0 and wave length λ (*cf.* radar equation in Lexicon, (Drake and Reynolds 2012) eq. 3.14b): $D_{max} = \sqrt[4]{\frac{P_t \cdot {G_0}^2 \cdot \lambda^2 \cdot RCS}{P_{r_{min}} \cdot (4 \cdot \pi)^3}}$

dB: The unit decibel expresses the logarithmic ratio on base 10 between the transmitted power (P_t) and the received power (P_r). A proper calibration of the radar system allows expression of the power in dBm, using a standard reference of 1 mW: $P_{r,dBm} = 10 \cdot \log_{10}(P_{r,W}/1_{mW})$

Echo signature: The echo intensity of an object varies during its transit of the radar beam. The echo signature represents the temporal variation in echo intensity (*cf.* P_r in Lexicon). Fine scale temporal variations in echo intensity are due to small changes in the object's aspect and reflectivity properties.

Echo size [dBm]: Maximal echo intensity of an object as measured by the radar receiver (*cf.* P_r in Lexicon) after removing low amplitude variations in echo intensity with a low pass filter. The echo size depends on object properties (size, aspect, reflecting properties, etc.), radar properties (wave length λ, transmitted power P_t, antenna gain G_0), the distance to the radar, and properties of the atmosphere.

G_0 [dB]: The antenna gain is a measure which describes the extent to which the antenna directs the beam towards the main beam axis (*sensu* Drake and Reynolds 2012).

λ [m]: Length of the electromagnetic waves, calculated as the speed of light (c, about $3 \cdot 10^8$ m * s^{-1}) divided by the emission frequency (f, e.g. 9.4 GHz): $\lambda = \frac{c}{f}$.

Mie region: The relationship between the object size and the RCS depends on the electromagnetic wave length λ and can be described in three regions: optical region if object diameter >> λ, Mie region if object diameter ≈ λ, Rayleigh region if object diameter << λ. The wave length of the 9.4 GHz radar system used in this study is 3.2 cm (see Lexicon "wave length"). While the RCS of objects larger than ten centimetres diameter is proportional to its size (optical region), the RCS of objects ranging from one to ten centimetre is not proportional to the object size (Mie region) (see e.g. (Drake and Reynolds 2012), p. 53). For instance, an object of 5 cm may produce an RCS of 25 cm^2 (5.64 cm diameter), where as an object of 5.5 cm diameter may produce an RCS of 15 cm^2 (4.37 cm diameter). This phenomenon progressively increases with decreasing object size, and is particularly strong for objects between one to three centimetres with RCS up to four times the object size. In the Rayleigh region, the decrease of RCS is steeper than the decrease of the object size.

Monitored volume: Also known as radar coverage or isoechoic contour, the monitoring volume defines the maximal ranges for echo detection: the maximal detection distance D_{max}, as well as the effective beam width (*cf.* $Width_{beam}$ in Lexicon). The monitored volume depends on the object size, and increases with increasing object size.

MTR [bird * km^{-1} * h^{-1}]: Migration Traffic Rate is a standardised measure of bird movements (Lowery 1951, Liechti et al. 1995). It describes the number of birds crossing a virtual transect line of one kilometre within one hour. By considering flight altitude, subsets can be given for different height intervals. For example, the MTR of a period between t_1 and t_2 is the sum of the MTR-factors (s. below) multiplied by the ratio between an hour and the time period [hour] between t_1 and t_2: $MTR = \sum_{t_1-t_2} MTR_{factor} \cdot \frac{1}{t_1-t_2}$.

MTR_{factor}: The MTR-factor is defined as the ratio between the one kilometre transect line and the effective beam width $Width_{beam}$, at the object's distance and for the object's estimated size: $MTR_{factor} = 1000/Width_{beam}$. For example, MTR_{factor} equals five for a 200 m $Width_{beam}$. The MTR-factor indicates the individual contribution of each echo to the MTR: e.g. the sum of all MTR-factors within an hour and a given height interval provides the MTR (*cf.* MTR in Lexicon). The MTR-factor therefore accounts for the distance-dependent variation in monitored volume.

Object size [m^2]: Visual profile produced by an object. Reflectivity properties and aspect of the object in respect to the polarisation plane of the beam greatly influence the relationship between the actual object size and the measured RCS.

$P_{r_{min}}$ [dBm]: The detection threshold defines the minimal echo size for detection (*cf. STC*).

P_t [W]: The transmitted power P_t represents the peak in power transmitted in pulse radar. Pulse radar sequentially emits electromagnetic waves and then listens for the echoes. The electromagnetic waves are created in a magnetron, and transmitted via the antenna.

Radar equation: The radar equation defines the main relationship between the echo power received by the radar P_r [W], and properties or the radar (transmitted power P_t [W], antenna gain G_0 [dB], wave length λ [m]), the illuminated object properties (i.e. RCS [m^2]), and it's $distanc$e [m] from the radar antenna. The radar equation can be formulated as follows (Drake and Reynolds 2012) eq. 3.14a): $P_r = \frac{P_t \cdot {G_0}^2 \cdot \lambda^2 \cdot RCS}{64 \cdot \pi^3 \cdot distance^4}$.

Radiation pattern (antenna diagram): A diagram describing the transmission and receiving characteristics of an antenna for a specific electromagnetic wave length (e.g. X-band). It describes the direction (3D) dependent gain in transmitting and receiving power expressed in decibel (dB), as measured by the manufacturer.

RCS [m^2]: The Radar Cross Section describes the reflectivity properties of an object. The RCS is wavelength specific and depends among other things on the reflectivity properties of the object (Eastwood 1967, Drake and Reynolds 2012). Following the radar equation (see Lexicon), the received power P_r is the only object specific quantity measured by non-coherent radar transmitter. Therefore, the RCS can be calculated by correcting the echo size (as a measure of P_r) by the distance (Drake and Reynolds 2012, eq. 4.1): $RCS = \frac{P_r \cdot (4 \cdot \pi)^3 \cdot distance^4}{P_t \cdot {G_0}^2 \cdot \lambda^2}$. We obtain a true RCS only for echoes that transit through the centre of the beam; the RCS is underestimated for all other echoes.

STC_{dist} [m]: The Sensitivity Time Control is an adjustable sensitivity setting used to attenuate the received power of signal close to the antenna. The STC sets a time (or distance, since time multiplied by the speed of light gives a distance, e.g. 300 m is about 10^{-6} s) at which the signals are not attenuated any more. In many radar systems available on the market such a STC filter is implemented, as a distance-dependent function, generally unknown to the user. For proper quantifications of small objects, the function should be based on the radar equation (Eastwood 1967). STC filters usually act prior to the echo detection and can be further increased post-hoc.

Waveguide attenuation [dB]: Attenuation of the transmitted and received power by the waveguide

$Width_{beam}$ [m]: The effective beam width for echo detection depends on the object's reflective properties and its distance from the antenna. The variation of the beam width with the distance from the radar defines the monitored volume (Drake and Reynolds 2012). $Width_{beam}$ is calculated for a given object size and distance from the radar antenna, given the following radar parameters (transmitted power P_t, antenna gain G_0, wave length λ, waveguide attenuation, radiation pattern (see R-function "funMTRfactor" in Appendix F).

Introduction

The lowest one to two kilometres of the atmosphere host huge quantities of animal movements, often invisible to the human eye (La Sorte et al. 2015, Hu et al. 2016, Chilson et al. 2017, Bruderer et al. 2018). Increasing human aerial activities and the trend towards more and taller constructions increase the collision and mortality risks of these animals aloft (Loss et al. 2015). Thus, there is an increasing demand on monitoring these movements for environmental impact assessments (e.g. at wind farms). Radar systems provide an ideal tool to monitor the temporal and spatial patterns of animal movements locally (Bruderer 1997, Nilsson et al. 2018), as well as on a large scale (Gauthreaux et al. 2003, Chilson et al. 2012, Nilsson et al. this issue). Therefore, the significance and demand for quantitative radar studies on animal movements in the context of ecological or environmental impact assessment studies has increased considerably (Bridge et al. 2011, Bauer and Hoye 2014).

An accurate quantification of animal movements requires an adequate, but not easily accessible, knowledge of the monitored volume (Schmaljohann et al. 2008, Drake and Reynolds 2012, Larkin and Diehl 2012). In principal, radars transmit electromagnetic waves that propagate in a three-dimensional beam along a main axis. The shape and extent of the beam defines the volume of air monitored by the radar. The monitored volume can be estimated using the radar equation (see Lexicon, (Eastwood 1967), requiring information on radar parameters and reflectivity properties of the objects. Radar specific parameters (e.g. wave length λ, antenna shape) are readily provided by the manufacturer, but the access to information on adjustable sensitivity settings for echo detection [e.g. detection threshold $P_{r_{min}}$, sensitivity time control (STC_{dist}), see Lexicon] is not guaranteed. In addition to radar properties, the monitored volume strongly depends on the object's size (Schmaljohann et al. 2008). Large objects have a bigger monitored volume than smaller objects (Figure 1a): they are detectable at greater distances along the beam axis, and at wider distances from the beam axis, than smaller objects. However, the actual object size cannot be directly measured by radar. Radar registers the maximal echo intensity (echo size, see Lexicon). Because the echo size decays at a known rate with distance from the radar antenna (power law of four, see radar equation in Lexicon), we can correct the echo size for its distance and obtain a best approximation of the radar cross section (RCS, see Lexicon). The RCS is therefore the echo size corrected for the distance along the main axis, but the RCS is related to the object size only for objects that transit through the beam centre. Because the echo size decreases with increasing distance from the beam axis, objects illuminated in the periphery of the beam will appear smaller (have smaller echo size) than an object of the same size detected in the beam centre (Figure 1b). Therefore, the RCS is a minimal measure of the object size.

The frequency at which birds flap their wings is highly correlated with their body size, with larger birds flapping slower than small ones (Pennycuick 2001, Bruderer et al. 2010). This relationship has also been shown in several insect groups (Drake and Reynolds 2012, Greenewalt 1962). The wingbeat frequency of a target can be estimated from the variation in echo intensity over time (echo signature, see lexicon) (Eastwood and Rider 1966, Bruderer et al. 2010, Bruderer and Joss 1969). Therefore, we can use the wingbeat frequency to estimate the size of the target/object, independently from the echo size (Figure 1c). The size distribution of measured targets can then be used to accurately estimate of the size-specific monitored volume for different taxa (Figure 1d).

In this study, we analysed six million echoes detected with a vertical-looking radar system (Nilsson et al. 2018), located at a range of sites along the avian African-Eurasian migratory flyway (from Sweden in the north, United Kingdom in the west, to Israel in the south-east), such that birds from a wide geographic range will have been sampled. We used features of the echo signature to classify each echo into four echo-types ("passerine", "wader", "unidentified-bird", and "non-bird"), and estimated the WBF (Zaugg et al. 2008). We first illustrate the influence of adjustable sensitivity settings on the number of detected bird and non-bird echo-types, and its consequences for the monitored volume. We then propose a quantitative framework to estimate the object sizes for echoes with similar wingbeat patterns, and test whether the estimated object sizes are consistent across large geographical ranges that likely differ in the species composition of migratory birds. Finally, we demonstrate the importance of accounting for size-specific monitored volume in order to accurately quantify the height distributions of animal movements aloft. This result highlights the importance of considering the size-specific monitored volume for each echo, and is an important step towards a truly quantitative estimation of animal movements using radar systems.

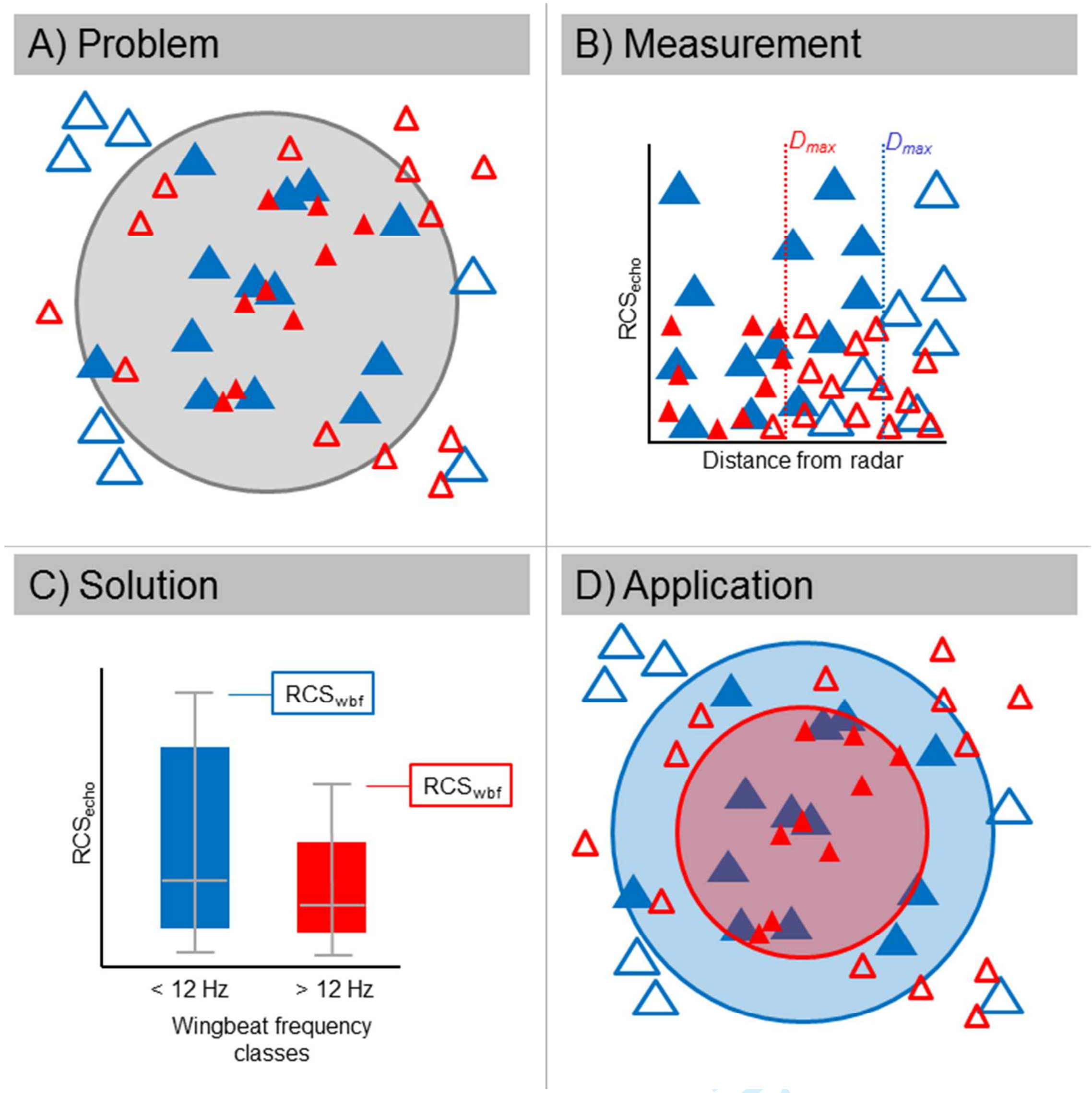

Figure 1: Research scheme. A) Most radar studies assume a maximum detection distance (monitored volume, grey disk) for all detected objects (filled symbols), irrespective of their size (object size: blue > red). However, many small objects remain undetected (open symbols) within the maximum detection distance (red-open symbols within the grey circle). B) Radars detect echoes with large RCS further away than echoes with small RCS (maximal detection distance D_{max} indicated by the vertical dotted line with the respective colour). Because the estimated RCS of objects decreases with increasing distance from the beam axis, the RCS of objects of different size overlap in the low ranges. Therefore, the actual size cannot be directly measured, but C) the wingbeat frequency (WBF) can be used to separate large from small birds (Pennycuick 2001). The upper range of the RCS distributions (RCS_{wbf}) should to be closest to the true RCS due to individuals flying across the centre of the beam. D) Applying RCS_{wbf} results in size specific detection monitored volume (blue and red disks).

Methods

Echo detection, classification and wingbeat frequency

We used a modified X-band marine radar (Bridgemaster©, 25 kW, 9.4 GHz, wavelength ca. 3.2 cm) with a vertical-looking 20dB Horn antenna (17.5 ° nominal beam angle at -3 dB; Swiss BirdRadar Solution AG, swiss-birdradar.com). We used 70 ns short-pulse emission for a range resolution of 10 m and a maximal detection range of 1500 m. An automated software detects objects passing through the beam, and digitises the detected echo signals (sampling frequency = 425 – 450 Hz). The digitizer converts the received signal into dBm based on calibration measurements with a signal processing unit and a reference power of 1 mW. The echo signature describes the temporal variation of the echo intensity (see Lexicon). The echo intensity is greatest when objects transit closest to the beam centre. The echo intensity also varies in relation to changes in the aspect of the object, such as the wingbeat movements of birds. To remove the small variations in echo intensity induced by changes in aspect, we apply a low pass filter (Chebyshev type I filters of order 5 with nominal band-pass limit set to 0.5 Hz) on the echo signature to identify the maximal echo intensity (hereafter referred to as echo size [dBm]). Once corrected for the distance according to the radar equation, the echo size is expressed as the radar cross section (RCS [m^2], see Lexicon), assuming objects have the same reflectivity properties. The echo size and its related RCS can strongly depend on the aspect of the animal in relation to the beam orientation (Edwards and Houghton 1959, Bruderer and Joss 1969, Mirkovic et al. 2016). Since vertical-looking radars illuminate animals from below ("ventral aspect"), the influence of aspect variation in a low-pass-filtered RCS is low and thus neglected in this study. For a given object size, the RCS is maximal when the object passes through the beam axis, and minimal at the detection threshold at the periphery of the beam.

We used supervised learning to automate manual echo classification and manual assessment of wingbeat frequency (WBF). A band-pass filter (Chebyshev type I filters of order 5 with nominal band-pass limits set to 4 and 180 Hz) removed high frequency signal oscillations partly due to the 0.8 Hz rotation of the antenna. We used features derived from the echo signature (detailed features in Appendix Table A1) and trained random forest classifiers to group the echoes into four echo-types ("passerine", "wader", "unidentified-bird", and "non-bird"; Zaugg et al. 2008). Class probabilities are calculated for each echo, and the class with the highest probability is assigned to the echo. We re-classified echoes with class probabilities for passerine-type and wader-type lower than 0.5 as unidentified-bird-type. Non-bird echoes are insects and other non-determined objects. We assessed the WBF [Hz] with a random forest regression model trained with manually confirmed WBF values, and features extracted from band-pass echo signatures (detailed features in Appendix Table A1). For each estimated WBF, a credibility factor is provided as the proportion of regression trees reaching close consensus. Cross validation of estimated WBF with manually determined WBF based on expert knowledge shows Pearson correlation coefficient of 0.976 (on a subset of echoes with credibility factors ≥ 0.5). Because of the low-band pass filter (see above), the trained classifier cannot determine WBF below 4 Hz. We restricted the WBF range to 25 Hz for birds (maximal known WBF for European birds, see Bruderer et al. 2010) and to WBF with credibility factors larger than 0.5.

Data

We used data from 11 monitoring sites (Table 1): Sempach (Switzerland (CH), year round), Col de Bretolet (CH, autumn), Geneva (CH, spring), Moelle (Sweden (SE), autumn), Sivry (France (FR), autumn), Herzeele (FR, autumn), Upper Galilee (Israel (IL), spring), Arava (IL, spring and autumn), Lower Galilee (IL, spring and autumn), Carmel (IL, spring and autumn), and Falmouth (United Kingdom (UK), year round). During the course of these monitoring campaigns, the deployed radars registered 6,460,205 echoes, of which 660,200 were "passerine-type" echoes (79.5% with WBF), 96,337 were "wader-type" echoes (97.8% with WBF), 1,136,481 were "unidentified-bird-type" echoes (44.1% with WBF), and 4,567,187 echoes were classified as "non-bird-type". This latter category undoubtedly consisted largely of insects, which at times can be hugely abundant in the atmosphere (Drake and Reynolds 2012; Hu et al. 2016). We also note that wader-type echoes may also include echoes from bats (Bruderer and Popa-Lisseanu 2005). The WBF of bats range between 5 to 12 Hz (similar values to the bird species classified as wader-type), and bats follow similar WBF-body size relationship as birds (Bullen and McKencie 2002, Norberg and Norberg 2012). Further knowledge on cross-validated echo signatures may enable disentanglement of wader-type bird-echoes from bat-echoes. The monitoring campaigns differed in sensitivity settings: STC_{dist} ranged from 100 m to 500 m, and detection threshold $P_{r_{min}}$ ranged from -100 dBm to -90 dBm.

Table 1: Overview of the 11 sites with radar monitoring: the geographic location (CH: Switzerland, SE: Sweden, FR: France, IL: Israel) and the monitoring period are provided, however the operation of the radar during these periods was not always continuous.

Site	Latitude, Longitude	Altitude [m asl]	Start	End	Monitoring days (hours)
Sempach (CH)	47.1, 8.2	450	Mar. 2016	Jun. 2017	504 (9707)
Geneva (CH)	46.2, 6.0	395	Mar. 2017	Jun. 2017	72 (1569)

Col de Bretolet (CH)	46.2, 6.8	1200	Aug. 2016	Oct. 2016	72 (1325)
Moelle (SE)	56.3, 12.5	70	Sep. 2015	Nov. 2015	62 (1384)
Herzeele (FR)	50.9, 2.5	10	Aug. 2016	Oct. 2016	59 (1124)
Sivry (FR)	48.8, 6.2	250	Oct. 2016	Nov. 2016	47 (967)
Upper Galilee (IL)	32.9, 35.2	350	Sep. 2015	Nov. 2015	66 (1417)
			Feb. 2016	May 2016	95 (2132)
Arava (IL)	30.7, 35.0	15	Mar. 2016	May 2016	81 (1911)
			Aug. 2016	Nov. 2016	79 (1795)
Lower Galilee (IL)	32.6, 35.4	115	Mar. 2016	Jun. 2016	77 (1799)
			Aug. 2016	Nov. 2016	92 (2168)
Carmel (IL)	32.6, 35.1	250	Aug. 2016	Nov. 2016	94 (2144)
Falmouth (UK)	50.2, -5.1	120	Mar. 2015	Mar. 2017	483 (5993)

Analyses

Influence of sensitivity settings and object size on monitoring volume

Using calculations based on the radar equation (see Lexicon), we illustrate the influence of adjustable sensitivity settings (detection thresholds $P_{r_{min}}$: -93 dBm, -87 dBm) and object diameter (5 cm or 15 cm) on the monitored volume, especially on the maximum detection distance (D_{max}), and on MTR-factors. The MTR-factor is the ratio between a 1-km transect line and the effective beam width at the distance of detection (see Lexicon). The MTR-factors thus account for size-specific and distance dependent variation in effective beam width, and represent contribution of each echo to MTR. We compute the effective beam width for each 1 m using an R-function based on the radar equation (Appendix F, R-function "funMTRfactor") and the following parameter: STC_{dist} 300 m, P_t 20 kW, and waveguide attenuation 0 dB. We further report the median of MTR-factors per 50 m distance bin.

Influence of sensitivity settings on number of detected echoes

We investigated the influence of adjustable sensitivity settings on the number of detected echoes for each echo-type. We applied the following post-hoc (i.e. after echo detection) sensitivity settings: $P_{r_{min}}$ of -90 dBm, -87 dBm, -83 dBm, and STC_{dist} of 500 m. We used all data monitored with a maximal $P_{r_{min}}$ -93 dBm and STC_{dist} 300 m and we report changes in number of echoes detected for each echo-type: passerine, and non-bird.

An increase of three dB of the detection threshold $P_{r_{min}}$ (a logarithmic scale) corresponds to a two fold increase in the required echoed energy for detection. With an increase of the detection threshold $P_{r_{min}}$, only echoes with an echo size larger than the post-hoc detection threshold remain in the dataset. Within the STC range, when the $distance$ [m] of the object from the radar antenna is smaller than STC_{dist} [m], the effective threshold $P_{r_{\min|stc}}$ [dBm] is higher than the detection threshold settings $P_{r_{min}}$ [dBm]:

$$P_{r_{\min|stc}} = \begin{cases} P_{r_{min}} - 40\,log_{10}(distance/STC_{dist}), & distance < STC_{dist} \\ P_{r_{min}}, & distance \geq STC_{dist} \end{cases} \quad \text{(Eq. 1)}$$

While $distance < STC_{dist}$, the STC-function effectively sets a minimal RCS for detection RCS_{min}. Indeed, reformulating the STC-function in W (*cf.* dB in Lexicon) gives $P_{r_{\min|stc,W}} = P_{r_{min,W}} \cdot \frac{STC_{dist}{}^4}{distance^4}$ (Eq. 2); Eq. 2 inserted into the radar equation (*cf.* RCS in Lexicon) further gives: $RCS_{min} = \frac{P_{r_{\min|stc,W}} \cdot (4 \cdot \pi)^3 \cdot distance^4}{P_{t,W} \cdot G_0{}^2 \cdot \lambda^2} = \frac{P_{r_{min,W}} \cdot (4 \cdot \pi)^3 \cdot STC_{dist}{}^4}{P_{t,W} \cdot G_0{}^2 \cdot \lambda^2}$ (Eq. 3). Therefore, RCS_{min} is independent on the detection distance. With an increase of the STC, only echoes with a RCS larger than or equal $to\ RCS_{min}$ remain in the dataset.

Determination of object size using wingbeat frequency

We estimate the object size of birds for each echo type and WBF intervals of 2 Hz. We report the 0.9- and 0.95-quantiles of the RCS distribution for each echo-type and 2 Hz WBF intervals [$object\ diameter = 2 \cdot (RCS/\pi)^{1/2}$), assuming an ideal spherical shape]. The species composition likely differs between the different geographical areas, and during spring and autumn migration events. We investigated whether the geographical region influences the observed RCS distributions. We used passerine-type echoes only because they are classified with high credibility, abundant on each site and cover the entire range of WBF. We tested the dependency of the 0.9-quantile of the RCS (transformed as $object\ diameter$, see above; using the 0.95-quantiles lead to quantitatively similar results) on WBF 2-Hz interval (as ordered factors), adding the site identity as a random intercept in linear mixed-effects models as implemented in the "lme4" R-package (Bates et al. 2015, R-version 3.4.3), assuming a Gaussian distribution of the residuals.

Distance distribution corrected for size specific monitored volume

To demonstrate the influence of MTR-factors on the estimate of migration intensity, we compared the distance distribution of the detected echoes with the distance distribution of MTR-factors. For each type of bird echo and WBF, we used the 0.90-quantile distribution of RCS (analyses with the 0.95 quantile were quantitative similar). The calculation of MTR-factor for each echo requires the following information: the estimated object size (0.90-quantile distribution of RCS per echo type and 2 Hz WBF interval, see Appendix Table A2), the distance (echoes are binned into 50 m distance intervals), the effective detection thresholds $P_{r_{min}}$ (see Eq. 1), the transmitted power P_t specified by the radar type, and the radiation pattern (see Lexicon) as provided by the antenna manufacturer (Appendix F, R-function "funMTRfactor"). We calculated the MTR-factors for all bird echoes registered with maximum $P_{r_{min}}$ of -93 dBm and STC_{dist} of 300 m, so that echo detection is based on a radar beam of the same shape.

Results

Influence of sensitivity settings and object size on monitoring volume

An increase of the detection threshold by 6 dB reduced the effective beam area (planar projection of the monitored volume along the distance axis) by about 50% (Figure 2: $P_{r_{min}}$-93 dBm *vs.* -87 dBm, see also Table A3 in Appendix). In particular, the maximal detection distance D_{max} decreased from 1361 m ($P_{r_{min}}$ -93 dBm) to 949 m ($P_{r_{min}}$ -87 dBm) for objects of 15 cm, and from 765 m ($P_{r_{min}}$ -93 dBm) to 527 m ($P_{r_{min}}$ -87 dBm) for objects of 5 cm (Table A3, Figure 2). In contrast, an increase of STC_{dist} from 300 m to 500 m only had a minor effect on the beam area (<10 %, Table 3) and does not affect the maximum detection distance as long as the object is large enough to be detected within the STC range.

The MTR-factors are inversely proportional to the effective beam width (see Lexicon). Setting higher detection threshold $P_{r_{min}}$ reduces the maximal detection distance D_{max}, and the MTR-factors above D_{max} are undefined and set equal to zero. Within D_{max}, setting higher detection threshold or STC reduces the effective beam width, therefore increases the MTR-factors at a given height. Similarly, at a given height, the MTR- factors of large objects are smaller than the MTR-factors of small objects.

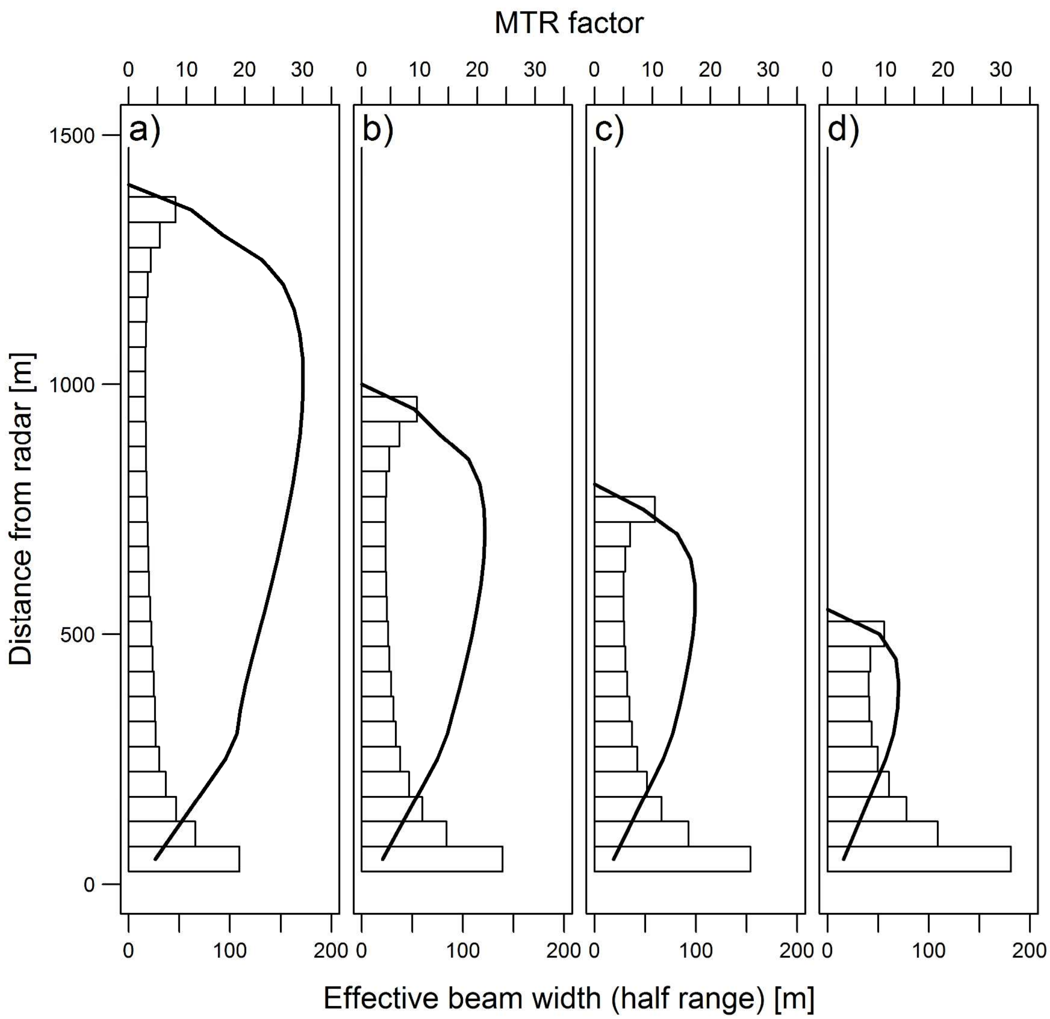

Figure 2: Effective beam width (half-range, solid lines, bottom x-axis) and MTR-factors (bars, 50 m distance bin, top x-axis) in relation to the distance for a) -93 dB $P_{r_{min}}$ and 15 cm object diameter (RCS = 0.0177 m^2), b) -87 dB $P_{r_{min}}$ and 15 cm object diameter, c) -93 dB $P_{r_{min}}$ and 5 cm object diameter (RCS = 0.0020 m^2), d) -87 dB $P_{r_{min}}$ and 5 cm object diameter. Further parameters to calculate the effective beam width: STC_{dist} 300 m, P_t 20 kW, and waveguide attenuation 0 dB (see R-function in Appendix).

Influence of sensitivity settings on number of detected echoes

An increase of the detection threshold and STC lowers the measurement sensitivity and reduces the number of detected echoes (Table 2, Figure 3). Obviously, a reduction of the sensitivity increases the minimal RCS for detection RCS_{min} (Table 2). In terms of echo detection, the effects of an increase of the detection threshold or of the STC differ (Figure 3). By increasing the STC, small objects, especially echoes classified as non-bird type, are reduced considerably. The proportion of non-bird echoes decreases from 59% (Table 2: STC_{dist} 300 m, $P_{r_{min}}$ -93 dBm) to less than 20% of the detected echoes (Table 2: STC_{dist} 500 m, $P_{r_{min}}$ -93 dBm). This 200 m increase of STC excluded 89% of the non-bird echoes, but only 28% of the passerines-type echoes. Increasing the detection threshold not only excludes small objects, it also reduces the monitored volume for any given object size. An increase in the detection threshold (-93 dBm to -90 dBm; Table 2) decreases the proportion of non-bird echoes to 42 % by excluding 67% of theses echoes, but this also leads to an exclusion of 30% of the passerine-type echoes.

Table 2: Influence of sensitivity settings (STC_{dist} and $P_{r_{min}}$) on the minimal RCS for detection RCS_{min}, the number of echoes, and the proportion of passerine-type and non-bird-type echoes. The total number of echoes also include wader-type and unidentified-bird-type echoes.

STC_{dist}[m]	$P_{r_{min}}$ [dBm]	RCS_{min} [cm^2]*	N. echoes	Proportion of echoes	
				Passerine	Non-bird (Insect)
300	-93	0.36	2915284	0.181	0.589
300	-90	0.72	1330121	0.279	0.423
300	-87	1.43	664900	0.381	0.224
300	-83	3.60	282270	0.418	0.064
500	-93	2.77	1108448	0.342	0.171
500	-90	5.54	455769	0.369	0.047
500	-87	11.04	193102	0.265	0.020
500	-83	27.74	52868	0.085	0.015

*using antenna gain G_0= 20 dB; transmitted power $P_{t,W}$ = 20 kW; see Eq. 3.

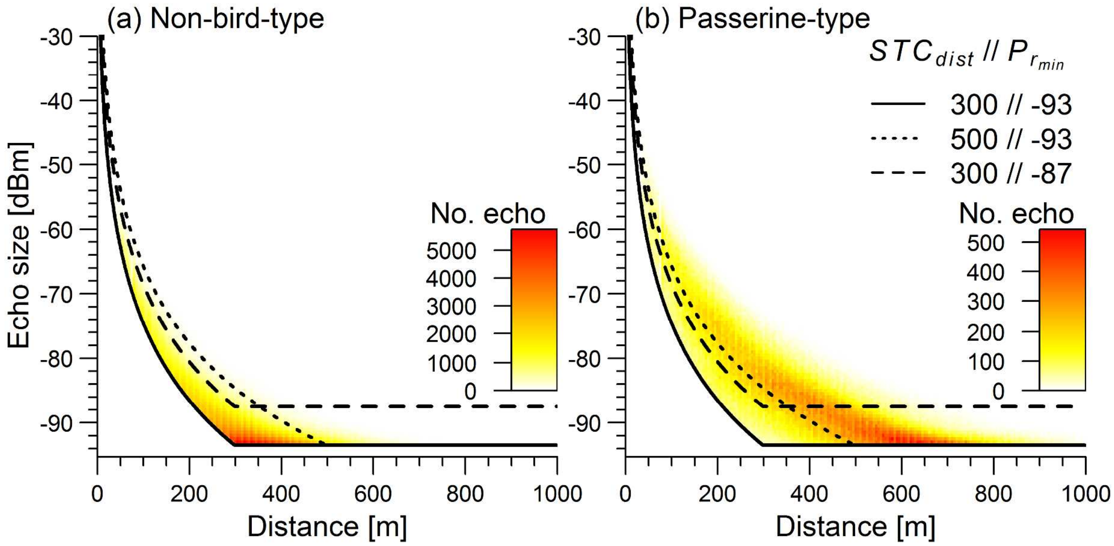

Figure 3: Echo size in relation to detection distance for a) non-bird-type echoes (mostly "insect") and b) passerine-type echoes. Lines delimit distance dependent detection thresholds $P_{r_{\min|stc}}$ (Eq. 1): i) STC_{dist} 300 m and $P_{r_{min}}$ -93 dBm (solid line), ii) STC_{dist} 500 m and $P_{r_{min}}$ -93 dBm (dotted line), and iii) STC_{dist} 300 m and $P_{r_{min}}$ -87 dBm (dashed line). Note the different scale of the number of echo between non-bird-type and passerine-type echoes.

Determination of object size using wingbeat frequency

The RCS decreased with increasing WBF for all three types of bird echoes (Figure 4). Considering echoes with similar WBF, the median RCS is smallest for passerine-type, generally highest for wader-type, whereas unidentified birds tend to show intermediate median values. The 0.9-quantile distributions of RCS parallel the 0.95-quantile distributions.

Wader-type echoes with low WBF (4 – 10 Hz) typically fell within the 12 – 13 cm diameter range. The wader-type echoes with 11 ± 1 Hz WBF had smaller 0.95 (or 0.90) RCS quantiles than echoes with 13 ± 1 Hz WBF. The relatively few wader-type echoes with WBF larger than 13 Hz only occurred in non-rotation mode and mostly occurred during night time. Passerine-type echoes with low WBF (4 – 12 Hz) had 0.95 RCS quantiles of 7 – 8 cm diameters. We observed a marked decrease in RCS between 11 Hz and 13 Hz WBF intervals. The RCS of passerines with WBF > 12Hz decreased steadily to a minimal 0.95-quantile diameter of 3.1 cm. Unidentified-bird-type echoes showed a steeper decrease in 0.95-quantiles between 5 Hz and 13 Hz WBF intervals than between 13 Hz and 25 Hz WBF intervals.

The 0.95-quantiles of RCS per 2 Hz WBF intervals for passerine-type echoes showed no differences between study site (using the 0.90 RCS quantiles were quantitatively similar). Between-site variance (0.22 ± 0.73) is about 20 times smaller than the averaged site value (Intercept 4.55 ± 0.08) and 10 times smaller than the decrease in RCS per two-Hertz (-2.34 ± 0.18; see also Figure S3 in Appendix E).

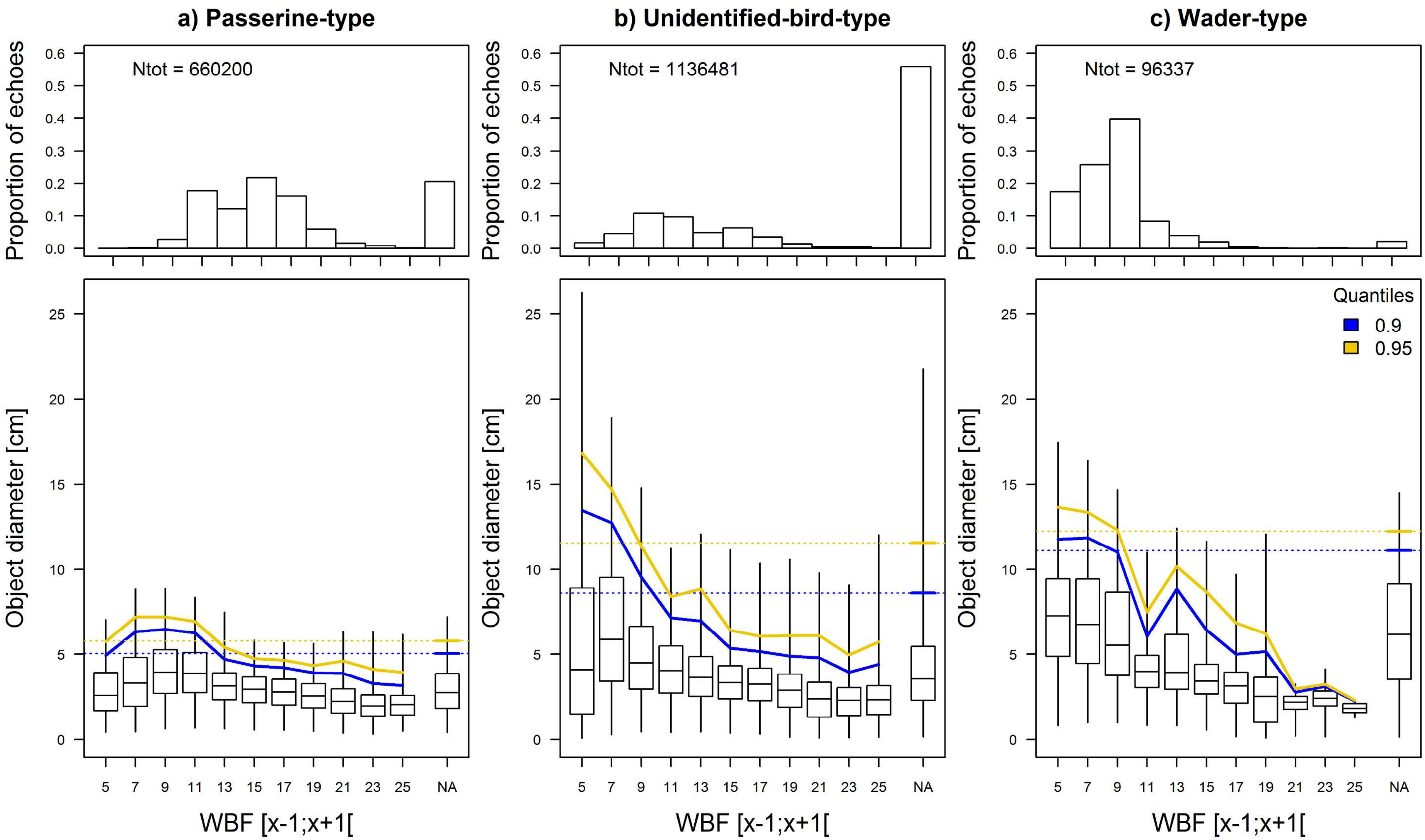

367
368 *[legend see next page]*

Figure 4: Distributions of registered object diameters (cm, $object\ diameter = 2 \cdot (RCS/\pi)^{1/2}$, assuming an ideal spherical shape) per 2 Hz WBF intervals for echoes of a) passerine-type, b) unidentified-bird-type, and c) wader type. Boxes show the 0.25 and 0.75 quantiles (vertical lines are the 0.01 and 0.99 quantiles). Coloured lines indicate the 0.9 (blue) and 0.95 (yellow) quantile of the distributions of object diameters per WBF-interval. Sample size (proportion of echo) indicated on top panels.

Distance distribution corrected for object-size dependent beam width

After correction for the monitored volume with MTR-factors, the height distribution of the MTR is lower than the height distribution of detected echoes (Figure 5). Fifty percent of the echoes were detected above the first 428 m (0.25-quantile: 266 m; 0.75-quantile: 597 m, Figure 5a), whereas 50% of the MTR occurred within the first 306 m (0.25-quantile: 167 m; 0.75-quantile: 499 m, Figure 5b). The lower distribution of MTR compared to the distribution of echo detection is due to the correction applied for a narrower beam width at short distance compared to mid-distances (Figure 2). The distance distributions of MTR depend on the maximal detection distance D_{max} of the different taxa, as calculated with the 0.90 RCS quantiles (see Appendix Table A2), although some echoes are detected further. According to the assumed object size per taxa, D_{max} of large passerines (passerine-type with WBF < 12 Hz) is 858 m, and D_{max} of small passerines echoes (passerine-type with WBF >12Hz) is 723 m (Figure 5). Beyond 723 m, the MTR-factors of passerine-type echoes with WBF > 12 HZ equals zero, and therefore beyond this limit movements of small-passerine are ignored.

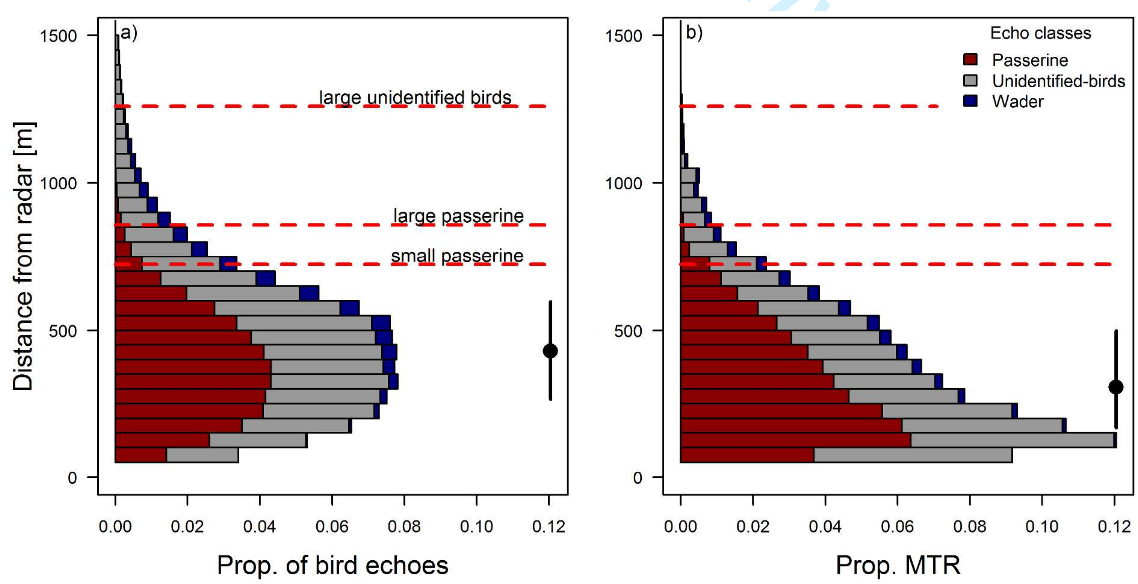

Figure 5: Distance distributions of a) echoes and b) MTR (MTR- factors according to the 0.90 RCS quantile for each echo type and WBF interval). Colours indicate echoes of different echo-types: red for passerine-type, grey for unidentified-bird-type, and blue for wader-type. The vertical black lines indicate the 0.25- and 0.75-quantiles, the dots indicate the 0.50-quantiles of the distance distributions. The horizontal red dashed lines indicate the maximal detection distances D_{max} ($P_{r_{min}}$ = -93 dBm, $P_{t,W}$= 20 kW, waveguide attenuation = 0 dB) for small passerine type (object diameter = 4.7 cm), large passerine type (object diameter = 6.5 cm), and large unidentified birds (object diameter = 13.5 cm). Above these lines, the MTR-factors equal zero for the respective echo groups.

Discussion

The typical assumption made by many radar operators, that all birds are detected within the maximal distance of bird detection, will lead to erroneous conclusions. This study provides a framework for the accurate quantification of avian movements with radar, taking account of the size-specific monitored volume. Using data collected from widely-separated areas across Europe, and a large range of flying animals, we estimated the size of a bird based on the WBF, independent of the echo size.

Influence of sensitivity settings

In this study, we demonstrate the effects of adjustable sensitivity settings on the detection of echoes of diverse types. Increasing the STC effectively removes small non-bird echoes. This is especially important because of the huge number of non-bird echoes (2/3 of all detected echoes), and a small probability of miss-classification can produce an elevated number of bird-type resulting from detection and misclassification of echoes from non-bird objects (insects). The STC also has the advantage of acting only within the distance set by the STC, so it does not reduce the maximal detection distance of the target objects. In contrast, increasing the detection threshold significantly reduces the surveyed volume. For instance, increasing the detection threshold substantially decreases the maximal detection distance of small birds. Beyond this distance, the radar only monitors movements of larger birds.

When possible, sensitivity settings should be selected to maximise echo detection. For a quantitative monitoring of avian migration, sensitivity settings (i.e. STC and detection threshold) should be appropriately selected in order to monitor movements of small birds. Setting high STC values post-hoc can remove echoes from small birds in studies that focus on large birds only (e.g. geese).

Therefore, adjusting the STC is an effective tool to match the specific aim and target object of radar monitoring, and using the appropriate radar parameters then correct for differences in the surveyed volume.

Knowledge of radar parameters (wave length, peak of transmitted power, antenna gain, waveguide attenuation, and the radiation pattern) and adjustable sensitivity settings (detection threshold and STC) are a prerequisite for any quantitative radar monitoring. Moreover, regular calibration will ensure registering of accurate information on standardised echo properties such as the echo size and its derived RCS (Atlas 2002, Schmaljohann et al. 2008, Urmy and Warren 2017, May et al. 2017, Drake and Reynolds 2012). Unfortunately, popular radar systems operating with built-in analysis software may not provide information on radar parameters and adjustable sensitivity settings to the end-users. In addition, some end-users can only monitor the radar display, not being able to register any quantitative information on the echo size (Nilsson et al. 2018). Such black-box radar systems render difficult any quantitative assessment of animal movements. As demonstrated in this study, the striking effects of adjustable sensitivity settings on the number of detected echoes per echo-type render the calibration and report of these sensitivity settings essential for any quantitative radar measurement.

Determination of object size using WBF

We estimated the object size from the echoed RCS for each echo-type (passerine-type, wader-type, and unidentified-bird-type) and WBF (2 Hz intervals). The smaller RCS of echoes with high WBF compared to echoes with lower WBF corroborate the negative correlation between body size and WBF defined in allometric flight models (Bruderer et al. 2010, Pennycuick 2001). The fact that the estimated RCS are independent from the study site and season provides support to the general validity of using WBF to estimate the object size.

Using the 0.90- or 0.95-quantile of the RCS distributions provides bird size estimates close to experimental measurements on birds measured on the broad side (Edwards and Houghton 1959, Bruderer and Joss 1969, Vaughn 1985). Deviation from the relationship between the WBF and the related bird size can occur because of variation in flight behaviour. For instance, many passerine-type echoes with WBF lower than 8 Hz may originate from swallows performing flap-gliding flight instead of flap-bounding flight (Rayner 1985, Liechti and Bruderer 2002, Tobalske 2007). Passerines contribute to the large majority of inland avian migrations fluxes (Hahn et al. 2009), and probably the majority of the unidentified-bird-type echoes are from passerine birds. Changes in the orientation of the bird's body within the beam can induce important changes in echo intensity, masking the regular modulation of the echo intensity due to the wingbeat patterns. Unidentified-bird-type echoes do not show a clear wingbeat type and less than 50% of the echoes had a credible WBF. Nevertheless, compared to passerine-type echoes, the upper RCS distribution of unidentified-bird-types is larger, probably because unidentified-bird-type echoes also include echoes from large soaring birds and bird flocks, shifting the RCS distributions to larger quantiles. Consequently, the over-estimation of the 0.90 RCS quantiles for unidentified-bird-type echoes leads to smaller MTR-factors, and an underestimation of the standardised movement intensity (MTR). The maximal WBF of wader-type birds reaches 12 Hz, with the notable exception of quails *Coturnix coturnix* (16Hz, Bruderer et al. 2010) and other echoes with WBF > 12 Hz are probable miss classifications.

The RCS used in this study is not corrected for the decay in echo intensity with increasing distance from the beam axis. The rotation of the antenna on a slight nutated axis can allow the estimation of the angle between the entry- and exit-point of the object in the beam in relation to the beam centre. Assuming a straight flight, this angle can be used to calculate the closest distance between the object and the centre of the beam, and thus to correct the RCS accordingly (Drake and Reynolds 2012). This requires an accurate estimation of the beam width, and has not yet been implemented in the radar system used in this study. We here proposed a method to determine the RCS according to the WBF, independently of the position of the object within the beam.

A similar approach could estimate the monitored volume for insects. Insects also show strong relationships between WBF and body size (Drake and Reynolds 2012, Greenewalt 1962). However, this relationship only holds within particular taxonomic groups, as insect taxa differ very much in size and wing shape. The estimation of insects' RCS based on WBF thus requires more detailed echo classification, or knowledge on flight phenology.

Distance distribution corrected for object-size dependent beam width

After correction for the monitored volume, the height (i.e. distance for a vertical looking antenna) distribution of the migration intensity is lower than if only reporting the height distribution of detected echoes. For instance, 50 % of the detected echoes were above 428 m agl, and after correction for the variation in monitored volume, 75 % of the animal movement intensity occurred below 499 m agl and even 50 % of the animal movement intensity occurred below 306 m agl. The differences in the height distribution of echoes and MTR highlight the potential misleading evaluation of collision risks of animals with human made structures such as wind turbines, bridges or power lines. In that regard, it is crucial that impact assessment studies accurately quantify the intensity of animal movements.

This article demonstrates the importance of reporting standardised movements such as MTR to avoid detection biases. Equally important is to report the maximal detection ranges (see Figure 5) because important migration intensity can occur at high altitude (reviewed in Bruderer and Peter 2017, Bruderer et al. 2018), far above the maximal detection range of a particular monitoring scheme. Quantitative information on high migration events can be retrieved using longer pulse emission that increase the maximal detection distance (with the use of lower detection threshold $P_{r_{min}}$). Alternatively, the increasing availability of weather radar data can complement height distribution retrieved from small scale radar systems (Nilsson et al. 2018).

Conclusions

Radar systems are valuable tools for the monitoring of aerial animal movements, but the results may suffer from important biases when the registered data is not processed adequately. In line with recent publications which detail adequate procedures (Schmaljohann et al. 2008, Drake and Reynolds 2012, Urmy and Warren 2017, May et al. 2017, Larkin and Diehl 2012) we hope that this publication will help to improve the scientific quality of radar monitoring.

We demonstrate the importance of accurately quantifying animal movement intensities, in particular for impact assessment studies of human-made structures (Aschwanden et al. 2018), or more generally to ecological studies of bioflows (Hu et al. 2016). Fixed-beam radar systems have the great advantage of being able to retrieve detailed information on the registered echoes, such as the WBF. We show how the WBF can be used as an independent measure of the body size of the animal, and how this taxa-specific RCS provides the most accurate estimation of the surveyed volume. When information on WBF is missing, expert knowledge on the body size (and its estimated RCS) can allow the estimation of the surveyed volume. Together with specific information on radar parameters (transmitted power, antenna gain, wave length, radiation pattern) and sensitivity parameters (detection threshold, STC), information on the taxa specific RCS are essential for any quantitative monitoring of animal movement and should always be made available and reported.

Contributions

BS and FL conceived the study. BS, MB, SCV, JWC collected the data. BS, FL, SZ conducted the analyses. BS wrote the manuscript with substantial contributions from all authors.

Data availability

Data used for this study are deposited on Zenodo: [doi upon acceptance]

Acknowledgements

This study was only possible thanks to the support of Daniel Früh, Dominik Kleger, Herbert Stark, Thomas Steuri, and Gregory Wills. We thank Cecilia Nilsson and two anonymous reviewers for their insightful comments that helped to further improve the quality of this article. We acknowledge the financial support of COST – European Cooperation in Science and Technology – through the Action ES1305 'European Network for the Radar Surveillance of Animal Movement' (ENRAM) for facilitating international collaboration.

References

Aschwanden, J. et al. 2018. Bird collisions at wind turbines in a mountainous area related to bird movement intensities measured by radar. – Biol. Conserv. 220: 228–236.

Atlas, D. 2002. Radar calibration: some simple approaches. – Bull. Amer. Meteor. Soc. 83: 1313–1316.

Bates, D. et al. 2015. lme4: Linear mixed-effects models using Eigen and S4. R package version 1.1--7.

Bauer, S. and Hoye, B. J. 2014. Migratory animals couple biodiversity and ecosystem functioning worldwide. – Science 344: 1242552.

Bridge, E. S. et al. 2011. Technology on the move: recent and forthcoming innovations for tracking migratory birds. – BioScience 61: 689–698.

Bruderer, B. 1997. The study of bird migration by radar. Part 2: Major achievements. – Naturwissenschaften 84: 45–54.

Bruderer, B. et al. 2010. Wing-beat characteristics of birds recorded with tracking radar and cine camera. – Ibis 152: 272–291.

Bruderer, B. et al. 2018. Vertical distribution of bird migration between the Baltic Sea and the Sahara. – J. Ornithol. 41: 282.

Bruderer, B. and Joss, J. 1969. Methoden und Probleme der Bestimmung von Radarquerschnitten freifliegender Vögel. – Rev. suisse Zool. 76: 1106–1118.

Bruderer, B. and Peter, D. 2017. Windprofit favouring extreme altitudes of bird migration. – Ornithol. Beob. 114: 73–86.

Bruderer, B. and Popa-Lisseanu, A. G. 2005. Radar data on wing-beat frequencies and flight speeds of two bat species. – Acta Chiropterol. 7: 73–82.

Bullen, R. D. and McKencie, N. L. 2002. Scaling bat wingbeat frequency and amplitude. – J. Exp. Biol. 205: 2615–2626.

Chilson, P. B. et al. 2012. Radar aeroecology: exploring the movements of aerial fauna through radio-wave remote sensing. – Biol. Lett. 8: 698–701.

Chilson, P. B. et al. (eds.) 2017. Aeroecology - Springer International Publishing.

Drake, V. A. and Reynolds, D. R. 2012. Radar entomology. Observing insect flight and migration - CABI.

Eastwood, E. 1967. Radar Ornithology - Methuen.

Edwards, J. and Houghton, E. W. 1959. Radar echoing area polar diagrams of birds. – Nature 184: 1059.

Gauthreaux, S. A. et al. 2003. Using a network of WSR-88D weather surveillance radars to define patterns of bird migration at large spatial scales. – In: Berthold, P. et al. (eds.), Avian migration. Springer, pp. 335–346.

Greenewalt, C. H. 1962. Dimensional relationships for flying animals. – Smithsonian Miscellaneous Collections 144.

Hahn, S. et al. 2009. The natural link between Europe and Africa - 2.1 billion birds on migration. – Oikos 118: 624–626.

Hu, G. et al. 2016. Mass seasonal bioflows of high-flying insect migrants. – Science 354: 1584–1587.

La Sorte, F. A. et al. 2015. Seasonal changes in the altitudinal distribution of nocturnally migrating birds during autumn migration. – R. Soc. Open Sci. 2: 150347.

Larkin, R. P. and Diehl, R. H. 2012. Radar techniques for wildlife research. – In: Silvy Nova J. (ed.), Techniques for wildlife manual. The John Hopkins University Press, pp. 319–335.

Liechti, F. and Bruderer, L. 2002. Wingbeat frequency of barn swallows and house martins: a comparison between free flight and wind tunnel experiments. – J. Exp. Biol. 205: 2461–2467.

Loss, S. R. et al. 2015. Direct mortality of birds from anthropogenic causes. – Annu. Rev. Ecol. Evol. Syst. 46: 99–120.

May, R. et al. 2017. Performance test and verification of an off-the-shelf automated avian radar tracking system. – Ecol. Evol. 7: 5930–5938.

Mirkovic, D. et al. 2016. Electromagnetic model reliably predicts radar scattering characteristics of airborne organisms. – Sci. Rep. 6: 35637.

Nilsson, C. et al. 2018. Field validation of radar systems for monitoring bird migration. – J. Appl. Ecol. 278: 3074.

Norberg, U. M. L. and Norberg, R. Å. 2012. Scaling of wingbeat frequency with body mass in bats and limits to maximum bat size. – J. Exp. Biol. 215: 711.

Pennycuick, C. J. 2001. Speeds and wingbeat frequencies of migrating birds compared with calculated benchmarks. – J. Exp. Biol. 204: 3283–3294.

Rayner, J. M. V. 1985. Bounding and undulating flight in birds. – J. Theor. Biol. 117: 47–77.

Schmaljohann, H. et al. 2008. Quantification of bird migration by radar - a detection probability problem. – Ibis 150: 342–355.

Tobalske, B. W. 2007. Biomechanics of bird flight. – J. Exp. Biol. 210: 3135–3146.

Urmy, S. S. and Warren, J. D. 2017. Quantitative ornithology with a commercial marine radar: Standard-target calibration, target detection and tracking, and measurement of echoes from individuals and flocks. – Methods Ecol. Evol. 8: 860–869.

Vaughn, C. R. 1985. Birds and insects as radar targets: a review. – Proceedings of the IEEE 73: 205–227.

Zaugg, S. et al. 2008. Automatic identification of bird targets with radar via patterns produced by wing flapping. – J. R. Soc. Interface 5: 1041–1053.

Supplementary information

Appendix A) **Features used for the echo classification and WBD estimation**

Table A1: *Description of features used for the echo classification and WBF assessment.*

Feature category	**Description**	**Used for**
Fundamental Frequency Estimators (FFE)	These features are 'weak' estimators of the fundamental frequency of a signal. If WF pattern is absent, the feature still has a numeric value. If WF pattern is present, generally only a subset of the values are valid approximations.	Echo classifier and WFF estimator
FFE-prominence	These features estimate the prominence of the spectral peaks used for the FFE and can be understood as a rough metric of quality for these features	Echo classifier and WFF estimator
Radar Cross Section (RCS)	This is an estimator of Radar Cross Section i.e. a target's intrinsic reflectivity which is a crude approximation of a target's size. It often underestimates the actual size.	Echo classifier only
Relative Magnitude of Fluctuations	These features estimate the relative magnitude of fluctuations in target's reflectivity.	Echo classifier only

Appendix B) **Estimated object size**

Table A2: *Table of estimated object size from the 0.90 RCS quantile, assuming a spherical shape of the birds:* $object\ diameter = 2 \cdot (RCS_{0.90}/\pi)^{1/2}$.

WBF [Hz]	Object diameter [cm]		
	Unidentified-bird-type	Passerine-type	Wader-type
2	13.45	6.47	11.77
3	13.45	6.47	11.77
4	13.45	6.47	11.77
5	13.45	6.47	11.77
6	12.73	6.47	11.86
7	12.73	6.47	11.86
8	9.54	6.47	11.00
9	9.54	6.47	11.00
10	7.15	6.25	6.05
11	7.15	6.25	6.05
12	6.96	4.70	8.85
13	6.96	4.70	8.85
14	5.35	4.33	6.42
15	5.35	4.33	6.42
16	5.16	4.21	5.01
17	5.16	4.21	5.01
18	5.16	3.92	5.01
19	5.16	3.92	5.01
20	5.16	3.87	5.01
21	5.16	3.87	5.01
22	5.16	3.28	5.01
23	5.16	3.28	5.01
24	5.16	3.17	5.01
25	5.16	3.17	5.01
NA	8.61	5.05	11.10

Appendix C) **STC**

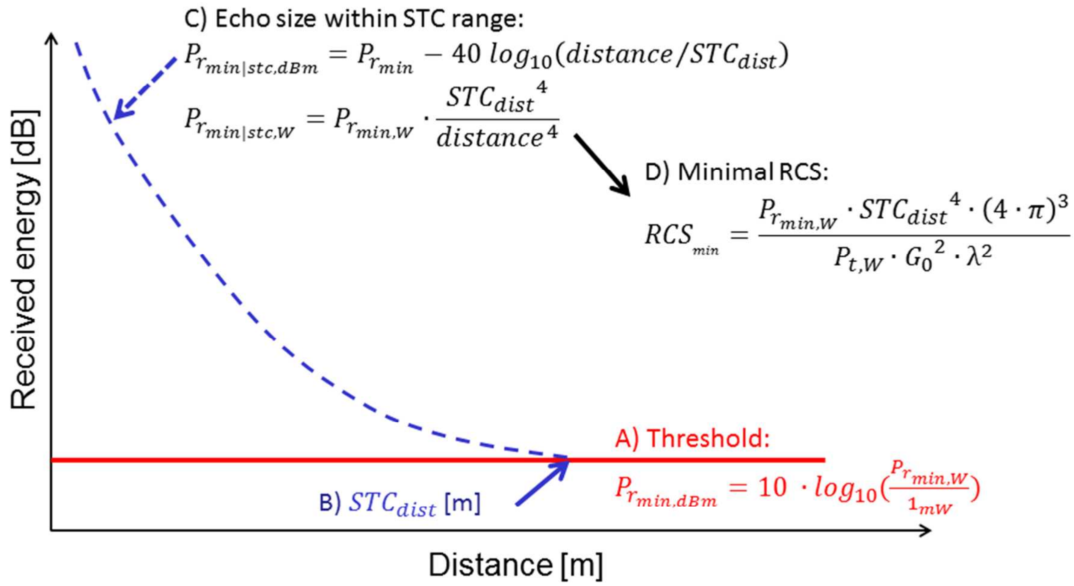

Figure S1: Calculation of STC filter. A given detection threshold $\boldsymbol{P_{r_{min,dBm}}}$ (A) and a given $\boldsymbol{STC}$ (B), set a distance-dependent echo size for detection (C, see Eq. 1). We obtain a RCS_{min} independent on the distance within the STC-range, using the radar equation $RCS = \frac{P_r \cdot (4 \cdot \pi)^3 \cdot distance^4}{P_t \cdot G_0{}^2 \cdot \lambda^2}$, and replacing P_r by $P_{r_{\min|stc,W}}$. Within the STC, all echoes with echo size smaller than $\boldsymbol{P_{r_{min,dBm}}}$ (dashed blue line) have an RCS smaller than RCS_{min} and are not detected, or removed post-hoc from the dataset.

Appendix D) **Monitored volume**

Table A3: Maximal detection distance $D_{max}$and effective beam area (and volume) depends on the sensitivity settings (threshold $P_{r_{min,dBm}}$ and STC) assuming a typical object size of 15cm-diameter, transmitted power P_t of 20 kW, and the antenna diagram provided by the manufacturer.

$P_{r_{min,dBm}}$	STC_{dist}	5 cm object diameter			15 cm object diameter		
		D_{max}	Total area	Total volume	D_{max}	Total area	Total volume
-93	300	765	111363	14614499	1361	350717	79758565
-90	300	636	77277	8506902	1137	245045	46913895
-87	300	527	53265	4897791	949	170624	27487956
-83	300	408	31613	2244713	744	105342	13462289
-93	500	765	102762	13016262	1361	336261	76233935
-90	500	636	67894	6910189	1137	233834	44451094
-87	500	527	40314	2974657	949	161713	25678177
-83	500	0	0	0	744	97073	11949402

Appendix E) **Influence of site identity on the RCS distributions**

Using 0.90-quantile of the RCS distribution, for Passerines only and finite WBF:

```
>lme1 = lme(ObjDiam_cm ~ wff_2Hz.of, random= ~ 1|campaignID.f, data=t.RCS,
control=list(maxIter = 100))
>summary(lme1)
Linear mixed-effects model fit by REML

Random effects:
 Formula: ~1 | campaignID.f
        (Intercept)  Residual
StdDev:   0.2230263 0.7332045

Fixed effects: ObjDiam_cm ~ wff_2Hz.of
                 Value  Std.Error  DF   t-value p-value
(Intercept)    4.546565 0.07850654 150  57.91321  0.0000
wff_2Hz.of.L  -2.342268 0.18330112 150 -12.77825  0.0000
```

The between-site variance (0.22 ± 0.73) is about 20 times smaller than the averaged site value (Intercept 4.55 ± 0.08) and 10 times smaller than the decrease in RCS per two-Hertz (-2.34 ± 0.18)

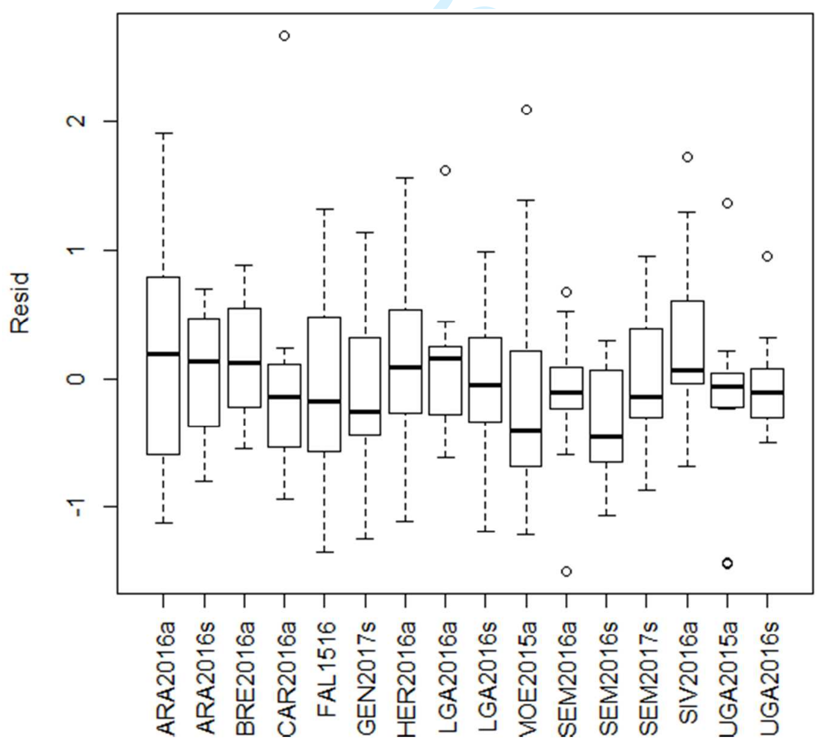

Figure S3: Between site variance of the square-root RCS corrected for the wingbeat frequency (sample size indicated on top).

Appendix F) **R-Functions**

funMinRCS

```
#*-**-**-**-**-**-**-**-**-**-**-**-**-**-**-**-**-**-**-**-**-**-**-**-**-**-**-**-**-**-*#
# original function snippet from Dominik Kleger, SwissBird Radar
TS = -93 # dBm as for Pr_min
Hmax = 300 # m as for STCdist
Psend = 22 # kW as for Pt
Again = 20 # dBi as for G0
funMinRCS <- function(TS=numeric(), Hmax=numeric(), Psend=numeric(), Again=numeric()){
  min_rcs  <-  (10^(TS/10)  *  10^-3  *  Hmax^4  *  (4*pi)^3)/((Psend*10^3)  *  (10^(Again/10))^2  *
(3*10^8/(9.4*10^9))^2)
  out <- min_rcs
}
```

funMTRfactor

```
#*-**-**-**-**-**-**-**-**-**-**-**-**-**-**-**-**-**-**-**-**-**-**-**-**-**-**-**-**-**-*#
# original function snippet from Dominik Kleger, SwissBird Radar
funMTRfactor = function(height, # distance of the object [m]
                        objectDiameter, # object diameter in cm (sphere)
                    waveguideAttenuation,  #  Attenuation  of  the  transmitted  and  received  power  by  the
waveguide [dB]
                        stc_level, # min dBm value possible for a given height, as for Pr_min_stc
                        Psend # in kW transmit power as for Pt
){

  # transform from kW to W
  transmitPower = Psend * 1000
  # compute back to radar cross-section in m^2 assuming spherical shape
  rcs =  pi*(objectDiameter/100)^2/4

  # MR1 specific parameters
  lut_phi_table = seq(0,90,5) # antenna diagram angle in Grad
  # diagram for "20dBiMR1"
  lut_lev_table = c(20, 19.5, 17, 10, 6, 0, -3, -10, -13, -17, -20, -20, -19, -19, -23, -30, -21, -25, -30)
   # antenna diagram Gain in dBi

  #- using flatten spline at phi=0
  xout <- unique(c(rev(seq(0, 90, 0.1)*-1), seq(0, 90, 0.1))) # use "unique" to avoid duplicated "0"
  int_res = spline(x = c(rev(lut_phi_table*(-1)),lut_phi_table), y = c(rev(lut_lev_table), lut_lev_table),
   xout = xout) # interpolate antenna diagram table
  #  plot(int_res$x,  int_res$y, ylab="level", xlab="phi", xlim=c(-100,100), col="green", type="l")
  #  points(lut_phi_table, lut_lev_table)
  #  abline(v=90)
  lut_lev = int_res$y[which(int_res$x >= 0)]
  lut_phi = int_res$x[which(int_res$x >= 0)]

  lut_lev_norm = lut_lev-lut_lev[1]
  antennaGain = 10^((lut_lev[1]-waveguideAttenuation)/10)
  f = 9.4e9 # electromagnetic wave frequency [Hz] or 9.4 GHz
  c = 3e8 # light speed
  # --> waveLength = c/f (see below in formula gainSTC)

  # ===================================================
  receiveLevelSTC = stc_level # alternatively use max(TS-40*log10(height/Hmax),  TS)
  receivePowerSTC = 10^(receiveLevelSTC/10)*1e-3
  gainSTC = sqrt(  (rcs*transmitPower*antennaGain^2*(c/f)^2) / ((4*pi)^3*height^4*receivePowerSTC)  )
  levelSTC = -10*log10(gainSTC)
```

```
  # values smaller than smallest antenna gain value -> set to value slightly higher than smallest antenna
   gain value
  index <- which(levelSTC <= lut_lev_norm[length(lut_lev_norm)])
  levelSTC[index] = lut_lev_norm[length(lut_lev_norm)] + 0.1
  # values bigger than biggest antenna gain value -> set value to zero
  index <- which(levelSTC >= lut_lev_norm[1])
  levelSTC[index] = 0

  # compute phiSTC
  phiSTC <- lapply(levelSTC, FUN=function(x){phiSTC = lut_phi[length(lut_lev_norm[lut_lev_norm > x])]})
  index <- which(levelSTC >= 0)
  phiSTC[index] <- 0
  index <- which(phiSTC < 0)
  phiSTC[index] <- 0
  phiSTC <- unlist(phiSTC)

  # get half-range
  halfRangeSTC = height*tan(phiSTC/180*pi) # convert to m
  # get full horizontal distance
  RangeSTC = 2*halfRangeSTC # m
  # get MTR-factor
  MTRFactor = 1000*(1/RangeSTC) # convert to "targets per meter" and then to "targets per km"
  MTRFactor[!is.finite(MTRFactor)] <- 0
  # ==================================================

  return( data.frame("mtrf"=MTRFactor, "RangeSTC"=RangeSTC, "halfRangeSTC"=halfRangeSTC) )
}
# end function body
```